ACOUSTIC WAVE PROPAGATION IN STANDING TREES −PART II. EFFECTS OF TREE DIAMETER AND JUVENILE WOOD[1]

Fenglu Liu

PhD
E-mail: liufenglu39@126.com

Houjiang Zhang*

Professor
School of Technology
Beijing Forestry University
Beijing, China
E-mail: hjzhang6@bjfu.edu.cn

Xiping Wang*†

Research Forest Products Technologist, PhD
USDA Forest Service
Forest Products Laboratory
Madison, WI
E-mail: xiping.wang@usda.gov

Fang Jiang

Associate Professor
E-mail: jf0602@bjfu.edu.cn

Wenhua Yu

Professor
School of Technology
Beijing Forestry University
Beijing, China
E-mail: yuwenhua56@sina.com

Robert J Ross

Assistant Director, PhD
USDA Forest Service
Forest Products Laboratory
Madison, WI
E-mail: robert.j.ross@usda.gov

Abstract. The objective of this study was to investigate the effects of tree diameter and juvenile wood on acoustic wave propagation in standing trees. Two-layer tree models with various diameters and proportions of juvenile wood were constructed to examine the effects of these two factors on propagation patterns and velocity of acoustic waves. The simulation results and analysis indicated that acoustic wave propagation in trees is dependent on both tree diameter and propagation distance. In the context of time-of-flight (TOF) acoustic measurement on standing trees with a test span of 1.2 m, when tree diameter is 10 cm or less, or

---

[1] The copyright of this article is retained by the authors.

slenderness is twelve or greater, wave propagates as quasi-plane waves in the tree trunk, and the tree velocity determined using the TOF method is then comparable to the log velocity measured using the acoustic resonance method. When tree diameter is 40 cm or larger, or slenderness is three or less, wave propagates as dilatational waves in the tree trunk; thus, the three-dimensional wave equation should be considered for wood property prediction. When tree diameter falls between 10 and 40 cm or slenderness falls between 3 and 12, wave propagation is in a transitional phase. Mathematical models were developed to convert the tree velocity in the transition mode to the resonance velocity. It was found that juvenile wood slows down the wave propagation. Our simulation results indicated that a 10% increase in the juvenile wood content resulted in a 113-m/s reduction in acoustic velocity. In addition, our analysis indicated that wave propagation in standing trees is controlled by the wood properties of entire cross section, not just the outerwood. Therefore, the wave velocity measured on standing trees reflects the global properties of the wood between the two measuring points.

Keywords: Acoustic waves, COMSOL multiphysics software, dilatational wave, plane wave, wave front, wave velocity, trees.

INTRODUCTION

The concept of using acoustic wave velocity as an effective measure of wood quality has been widely recognized in both forest products industry and forestry sector. A variety of acoustic instruments have been developed and applied to raw wood materials (logs and standing trees) and various wood products (lumber, veneer, laminated veneer lumber, glulam beams, etc.) as quality evaluation tools. In particular, the development of standing tree acoustic tools has opened the way for assessing wood quality of standing trees before harvesting, enabling management, planning, harvesting, and wood processing to be carried out in a way that maximizes the extracted value from the resource (Wang et al 2007a; Legg and Bradley 2016).

Acoustic wave methods employed for nondestructive evaluation of standing trees use a mechanical impact to generate low-frequency acoustic waves that propagate through the tree trunk, and then to measure the time of flight (TOF) of acoustic waves between two sensor probes (typically centered around tree's breast height spanning about 1.2 m). At the microstructure level, the acoustic wave velocity in a tree is controlled by the orientation of wood cells and structural composition, factors that contribute to stiffness and strength of wood. To date, research on using acoustic wave methods to assess wood quality of standing trees has been mostly experimental and limited to direct measurement of acoustic velocity in trees. Studies have shown that acoustic velocity of standing trees measured using a TOF technique (hereafter referred to as

TOF velocity) has a good linear relationship with the corresponding butt log velocity measured using a resonance acoustic technique (thereafter referred to as resonance velocity) (Lindström et al 2002; Joe et al 2004; Chauhan and Walker 2006; Wang et al 2007b). However, TOF-based tree velocity was found to be consistently higher than the resonance-based log velocity, which often leads to a skewed relationship, and subsequently an overestimation of wood stiffness (Andrews 2003; Hsu 2003; Chauhan and Walker 2006; Grabianowski et al 2006; Wang 2013; Legg and Bradley 2016).

Wang (2013) provided a thorough review and analysis of the acoustic measurements on trees and logs and elucidated two different mechanisms of acoustic measurements—the TOF method used for trees and the resonance acoustic method used for logs, which are believed to be the fundamental cause attributing to the tree velocity deviation. In log acoustic measurement, the acoustic waves propagate through the full length of a log and stimulate many, possibly hundreds of reflections from the ends of the log, resulting in a very accurate and repeatable velocity measurement. The acoustic waves in a log are considered to be dominated by a "rod" wave (Andrews 2003) governed by the one-dimensional wave equation:

$$C_0 = \sqrt{\frac{E_L}{\rho}}, \tag{1}$$

where C_0 is the longitudinal wave velocity in a rod, E_L is the longitudinal modulus of elasticity, and ρ is the mass density of the material.

By contrast, TOF acoustic measurement on a tree involves inserting two sensor probes into the tree trunk with a relatively short span distance, and acoustic waves can only be stimulated from the barkside of the tree through a pointed probe, resulting in a nonuniaxial stress state in wood material. Based on the analysis of experimental data, Wang et al (2007b) hypothesized that TOF measurement in standing trees is likely dominated by dilatational waves rather than one-dimensional "rod" waves. The theoretical dilatational wave velocity in an infinite or unbounded orthotropic medium can be obtained from the following equation:

$$C_L = \sqrt{\frac{1 - v_{RT}v_{TR}}{1 - v_{RT}v_{TR} - \alpha}\frac{E_L}{\rho}}, \qquad (2)$$

where C_L is the dilatational wave velocity; E_L is the longitudinal modulus of elasticity of the medium; v_{RL}, v_{LR}, v_{TL}, v_{LT}, v_{TR}, and v_{RT} are the Poisson's ratios in RL, LR, TL, LT, TR, and RT planes, respectively, of the orthotropic medium;

$$\alpha = 2v_{RL}v_{TR}v_{LT} + v_{TL}v_{LT} + v_{RL}v_{LR}$$

However, studies indicated that application of the dilatational wave equation for tree evaluation was affected by the diameter of the trees measured (Lasserre et al 2004; Wang et al 2004; Carter et al 2005). It is speculated that acoustic waves may travel in a tree as a quasi-plane wave when tree diameter is small, or as a dilatational wave when tree diameter is large. No diameter threshold has been discussed or proposed to differentiate two types of wave propagation modes in trees. The validity of the hypothesis of a "dilatational" wave for the TOF method needs to be further investigated in a systematic manner, whether by means of experiments or simulations.

The other possible cause for the tree velocity deviation is related to the stiffer wood zones—outerwood of the tree's cross section (Chauhan and Walker 2006; Grabianowski et al 2006; Mora et al 2009). Grabianowski et al (2006) conducted TOF measurements in logs and found that TOF

acoustic velocity showed a stronger correlation with the resonance velocity in the outerwood than that in the corewood. Chauhan and Walker (2006) stated that the higher velocity measured by the TOF tool is attributed, in part, to the fact that single-pass transit-time velocities are sensitive to the localized high stiffness of the outerwood lying in the wave propagation path between the two measuring points.

Field studies on nondestructive evaluation of plantation trees also indicated possible effects of stand age on tree acoustic velocities. The tree-to-log velocity ratio was found to increase as stand age increased. For instance, in evaluating 150 radiata pine trees in stands aged 8, 16, and 26 yr using a TOF tool, Grabianowski et al (2006) found an increasing trend of tree velocity with stand age. Wang et al (2007b) observed that younger age and smaller diameter of the radiata pine trees resulted in tree velocities that were much closer to log velocities than the 43-yr-old ponderosa pine. Similar trend was also reported by Chauhan and Walker (2006). Wang (2013) stated that this trend is in agreement with the current knowledge on tree growth; that is, as trees age, the outerwood gets stiffer because of the decreasing microfibril angle, and the proportion of mature wood in the cross section of a tree increases. As such, the overall mechanical properties improve with aging.

In this study, we attempted to simulate acoustic wave propagation in a virtual tree trunk through numerical simulation using COMSOL Multiphysics software (COMSOL, Inc., Burlington, MA) and examine the propagation patterns of longitudinal acoustic waves in standing trees. In part 1 of this report (Liu et al 2020), we found that with the consideration of orthotropic tree model and "free- and low-reflection" boundary conditions, the propagation of acoustic waves in a standing tree can be properly simulated using COMSOL Multiphysics software. The objective of this report (part 2) was to investigate the effects of tree diameter and proportion of juvenile wood on wave fronts and wave propagation velocity in standing trees. Two-layer tree models with various tree diameters and proportions of juvenile

wood were constructed to examine the effects of these two factors on propagation patterns and the velocity of acoustic waves.

MATERIALS AND METHODS

Tree Models

A tree trunk is composed of various materials present in concentric bands. From the outside of the tree to the inside are bark, vascular cambium, sapwood, heartwood, and the pith. To simplify tree modeling, we divided the cross section of a tree trunk into two distinct zones, juvenile wood and mature wood, with each assumed to be orthotropic.

The targeted plantation trees in our simulation work were 40-yr-old larch (*Larix principis-rupprechtii* Mayr) with a diameter at breast height (dbh) from 14 to 37.5 cm, a taper from 1 to 3 cm per meter, and the proportion of juvenile wood in 70%. The dbh and taper were based on the actual physical measurements on 50 sampled trees at a 40-yr-old fast-growing larch plantation in the Maojingba national plantation forest, Chengde, Hebei Province, China. The juvenile wood proportion was determined from the cross sections of three harvested larch trees from the same plantation. The observed radial variation for width of annual rings and latewood proportion in annual rings in the cross sections led to distinct boundaries between juvenile and mature wood.

The base tree model was set in a cylindrical form with a length of 2 m and a taper of 2.75 cm/m (Fig 1). The axial (*L*), radial (*R*), and tangential (*T*) directions of the tree model were defined as three principal axes *x*, *y*, and *z* in a Cartesian coordinate system. The model was further simplified with the following assumptions: 1) the cross section of a tree trunk is composed of two distinct zones, juvenile wood and mature wood; 2) each wood zone assumes orthotropic and homogenous medium; 3) no growth rings; and 4) no natural defects.

Tree model 1. The first series of simulations were run to investigate the effect of tree diameter
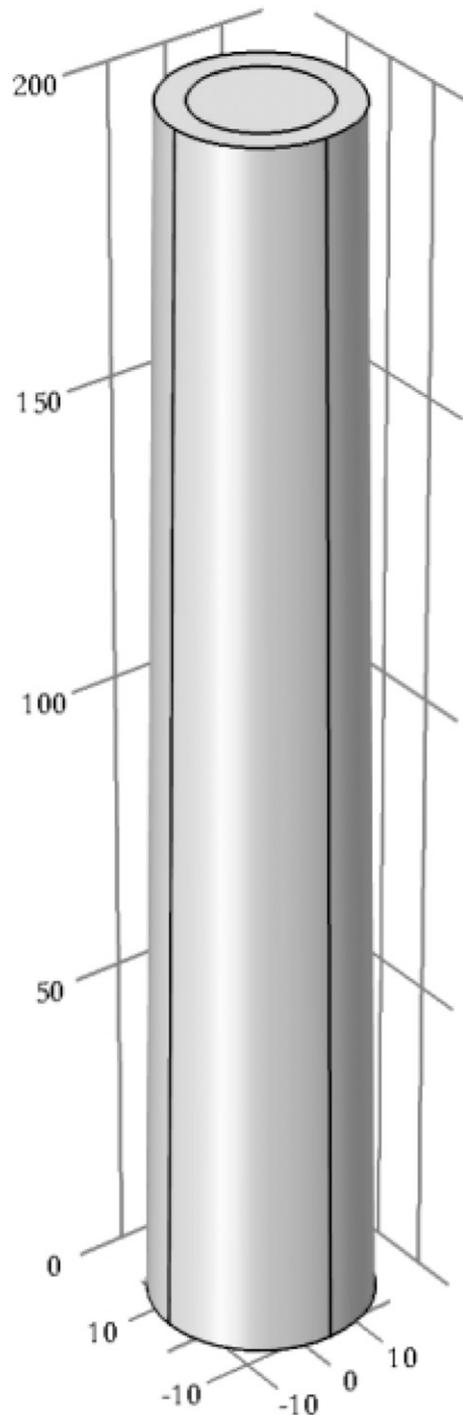

Figure 1.   Three-dimensional geometry model of a standing tree constructed using COMSOL software ($R_h = 70\%$, $D = 35$ cm, $d = 30$ cm).

on wave propagation patterns and propagation velocity in standing trees. In this scenario, the proportion of juvenile wood was kept constant as 70%; the large-end diameter of the tree model was set to different values: $D = 10, 20, 30, 40, 50, 70,$ and 90 cm (Fig 2). The geometrical variables of *Tree Model 1* are shown in Table 1.

Tree model 2. The second series of simulations were designed to examine the effect of the proportion of juvenile wood on wave propagation patterns and propagation velocity in standing trees. In this scenario, the diameter of the tree model was kept constant (35 cm for the large end and 30 cm for the small end), but the proportion of juvenile wood zone was set in a series of values, ie 40%, 50%, 60%, 70%, 80%, and 90% (Fig 3). The geometrical variables of *Tree Model 2* are shown in Table 2.

Material Properties

Nine elastic constants of green larch were determined through laboratory experiments in a previous study (Liu et al 2015). The wood specimens used to determine the elastic constants were cut from three larch logs harvested from a 40-yr-old larch plantation stand located in Chengde, China. The nine elastic constants and wood density of green larch are shown in Table 3. The average elastic constants and wood density of the specimens cut from the mature wood were used for the mature wood layer in the tree models. The average elastic constants and

wood density of the specimens cut from the juvenile wood were used for the juvenile zone in the tree models.

Numerical Simulations

We followed the same simulation procedures as used in part 1 of this report to carry out the numerical simulations. To mimic the actual impact pulse, we used the following half-sine pulse function as the impact load:

$$F(t) = \begin{cases} A\sin(2\pi ft), & t < (1/2f) \\ 0, & t \geq (1/2f) \end{cases}, \quad (3)$$

where A is the amplitude of the impact pulse and f is the frequency of the sine wave.

The amplitude of the pulse signal was calibrated to an impact force of 200 N. The width of the impact pulse was measured as 0.2 ms, which corresponds to a frequency of 2.5 kHz in a sine wave. $F(t)$ was further decomposed into two orthogonal components: $F_y(t)$ and $F_z(t)$, with the amplitude of each component being 141.4 N.

The initial displacement and initial velocity of the particles in the tree models were set to zero. Given the fact that a standing tree trunk is free from any constraints or load on the side surface, and the model domain is limited to a certain length (2.0 m in this article), the free boundary for the side surface and low reflection for the two ends were proved suitable for tree modeling and
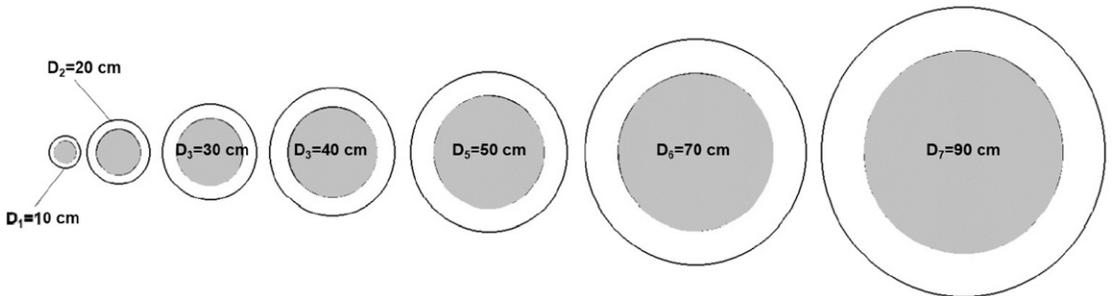

Figure 2.   Cross-sections of Tree Model 1 with large-end diameter varying from 10 cm to 90 cm and the juvenile wood kept constant as 70%.

Table 1. Geometrical parameters of Tree Model 1 for simulation runs of investigating tree diameter effect.

Geometrical parameter[a]	Simulation runs						
	1	2	3	4	5	6	7
L (cm)				200			
r_{JW} (%)				70			
D_i (cm)	10	20	30	40	50	70	90
d_i (cm)	5	15	25	35	45	65	85
D_{JWi} (cm)	7	14	21	28	35	49	63
d_{JWi} (cm)	3.5	10.5	17.5	24.5	31.5	45.5	59.5

[a] L, length of the tree model; D_i, large-end diameter of the tree model; d_i, small-end diameter of the tree model; D_{JWi}, large-end diameter of the juvenile wood zone; d_{JWi}, small-end diameter of the juvenile wood zone; r_{JW}, percentage of juvenile wood in the cross-section.

therefore adopted for the simulations in this report.

A swept method was applied to the tree model to get a reasonable number of grids. For the juvenile wood layer of the tree model, the largest and smallest elements of the end surface in the model were 3.5 cm and 0.004 cm, respectively, whereas for the mature wood layer of the tree model, the largest and smallest elements of the end surface in model were 2.5 cm and 0.004 cm, respectively. After the meshing of the end surface was completed, the swept method was used to extend the mesh to the whole tree model. The total number of meshes obtained from the tree model was up to 70,000.

RESULTS AND DISCUSSION

Effect of Tree Diameter on Wave Propagation

The numerical simulations using COMSOL Multiphysics software resulted in displacement contour maps at various time points. To visually illustrate the propagation patterns of acoustic waves in *Tree Model 1* with tree diameter as a variable, we developed a progression map of the wave fronts for each diameter variable by extracting the forefront contour surface from the

displacement contour maps at various time points: 100, 150, 200, 250, 300, 350, 400, 450, and 500 μs (Fig 4). This wave-front progression map is essentially a cluster of leading contour surfaces where the arrival time is the same at any point of surface (isochronous surface). Therefore, it illustrates the wave fronts in a tree model in a time sequence.

As an example, Fig 4(a) ($D = 10$ cm) best illustrates how an acoustic wave propagates in *Tree Model 1* over a long propagation distance relative to the tree diameter (20 diameters). The wave propagation patterns are generally consistent with what were reported in Part 1 of this report (Liu et al 2020). Initially, the side-induced wave spread over the tree's cross section with an ellipsoidal wave front in the impact direction. The propagation path then gradually shifted toward the longitudinal direction as the waves moved up, guided by the cylindrical shape of the tree model. As the waves propagated further up, both the curvature and gradient of the wave fronts gradually decreased. The wave front became a perfect plane at 12 diameters (1.2 m).

Comparing the wave-front progress maps of *Tree Model 1* in different diameters, it is evident that wave propagation in trees is not only affected by
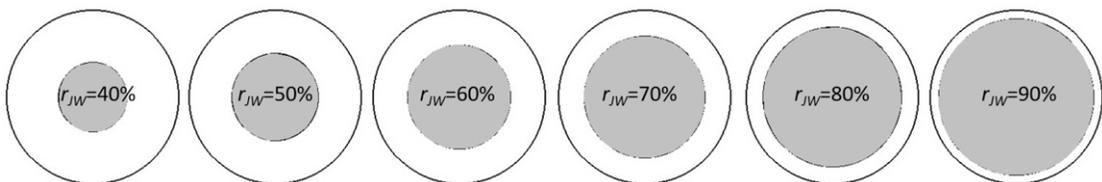

Figure 3.   Cross-sections of Tree Model 2 with juvenile wood ranging from 40% to 90%.

Table 2. Geometric parameters of Tree Model 2 for simulation runs of investigating juvenile wood effect.

Geometrical parameter[a]	Simulation runs				
	1	2	3	4	5
L (cm)	200	200	200	200	200
D (cm)	35	35	35	35	35
d (cm)	30	30	30	30	30
D_{JWi} (cm)	17.5	21	24.5	28	31.5
d_{JWi} (cm)	15	18	21	24	27
r_{JW} (%)	50	60	70	80	90

[a] L, length of the tree model; D, large-end diameter; d, small-end diameter; D_{JWi}, large-end diameter of the juvenile wood zone; d_{JWi}, small-end diameter of the juvenile wood zone; r_{JWi}, percentage of juvenile wood in the cross-section.

tree diameter but also dependent on propagation distance. We observed the following three distinctly different wave propagation patterns as the tree diameter changed from 10 cm to 90 cm.

Quasi-plane waves. In the 10-cm tree model, the acoustic wave initially spread over the cross section by propagating in an elliptical wave front. The wave front did not interact with the opposite side of the cross section within 3 diameters (3D) from the impact source; therefore, the wave can be considered "dilatational" in this region with a "three-dimensional" stress state (Meyers 1994). The wave front then quickly encountered the boundary which guided the waves moving upward. The wave front became a tilted oval surface interacting with the opposite side of the tree model after 3D, and then transformed to a tilted plane at about 6D. When the wave reached a propagation distance of approximately 10D, the wave front became almost a perfect plane, which may be considered purely "one dimensional" from this point forward. In the context of actual

tree measurement with 1.2-m test span, the wave propagates in mixed modes: as dilatational wave in 0-3D; in a transitional mode from 3D to 6D; as a quasi-plane wave from 6D to 10D, and then as a plane wave from 10D to 20D. The wave velocity at 1.2-m propagation distance was determined to be 3345 m/s from the simulation run, which is very close to the theoretical velocity (3335 m/s) of one-dimensional plane wave calculated from the average elastic constants and density of Chinese larch samples (Liu et al 2015). Therefore, the wave propagation in the 10-cm tree model can be practically treated as quasi-plane waves, and consequently, the wave behavior can be characterized by the one-dimensional wave Eq 1.

Waves in transition phase. In the 20-cm tree model, the wave appeared to propagate as a dilatational wave in the extent of 0-2D. After 2D, the wave front began to interact with the far side of the tree model and turned into tilted oval surfaces with large slopes (Fig 4[b]). As it traveled 6D (1.2 m), the wave front still maintained tilted with approximately 45°. In this scenario, the wave fronts within 1.2 m propagation distance were dominated by tilted oval surfaces, setting apart from both dilatational waves and plane waves. The wave velocity at 1.2 m propagation distance was determined to be 3426 m/s from the simulation run, which is 3% higher than the theoretical velocity of the one-dimensional plane wave (3335 m/s) and 12% lower than the theoretical velocity of the dilatational wave (3911 m/s). Similarly, in the 30-cm tree model, the wave propagated as a dilatational

Table 3. Elastic constants and density of juvenile wood and mature wood for green larch.

Wood zone	Modulus of elasticity (MPa)[a]		Modulus of rigidity (MPa)[b]		Poisson's ratio[c]		Density (kg·m^{-3})
Juvenile wood	E_L	6792	G_{RT}	415	υ_{RT}	0.76	—
	E_T	282	G_{LR}	427	υ_{LR}	0.21	500
	E_R	342	G_{LT}	375	υ_{LT}	0.28	—
	E_L	10,137	G_{RT}	556	υ_{RT}	0.81	—
Mature wood	E_T	388	G_{LR}	430	υ_{LR}	0.26	750
	E_R	915	G_{LT}	446	υ_{LT}	0.36	—

[a] E_L, longitudinal modulus of elasticity; E_T, tangential modulus of elasticity; E_R, radial modulus of elasticity.
[b] G_{RT}, shear modulus in *R-T* plane; G_{LR}, shear modulus in *L-R* plane; G_{LT}, shear modulus in *L-T* plane.
[c] υ_{RT}, Poisson's ratio of *R-T* direction; υ_{LR}, Poisson's ratio of *L-R* direction; υ_{RT}, Poisson's ratio of *L-T* direction.
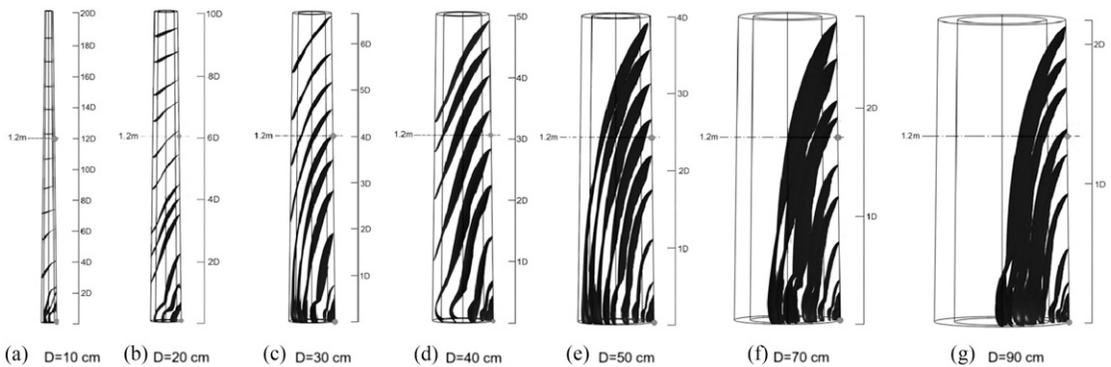
Figure 4.   Wave propagation patterns in Tree Model 1 illustrated by progression map of the wave fronts with diameter as a variable.

wave in the extent of 0-3D. The elliptical wave front at 1.2-m transit distance had an ellipticity of 4.25 and appears to reach the far end of the cross section. The wave velocity at 1.2-m propagation distance was determined to be 3780 m/s from the simulation run, which is 13.3% higher than the theoretical velocity of one-dimensional plane wave (3335 m/s) and 3.3% lower than the theoretical velocity of dilatational wave (3911 m/s). In both of these scenarios, the wave propagation mode should be treated as the transitional phase.

Dilatational waves. In the 40-cm tree model, waves appeared to propagate as dilatational waves beyond 3D (1.2 m) (Fig 4[d]). The wave velocity at 1.2-m propagation distance was determined to be 3899 m/s from the simulation run, which is close to the theoretical velocity of the dilatational wave (3911 m/s). Therefore, it can be certain that the wave propagation mode in the 40-cm model should be treated as dilatational waves. In the tree models of 50, 70, and 90 cm, the wave propagation as dilatational waves further expanded beyond 1.2-m and up to 2.0-m propagation distance (Fig 4[e]-[g]). The wave velocity at 1.2-m propagation distance was 3910, 3918, and 3918 m/s from the simulation runs, practically equal to the theoretical velocity of the dilatational wave (3911 m/s).

Considering all three patterns we just discussed, we found that the wave propagation mode in *Tree Model 1* is dependent on both tree diameter (D_i)

and propagation distance (L_i). The impulse acoustic waves initially spread over the cross section from the impact source as a dilatational wave (Phase 1); the waves then change to transitional waves with tilted oval surfaces and tilted planes (Phase 2); and the waves eventually transition to quasi-plane waves and pure plane waves (Phase 3) after traveling a sufficient distance, which depends on the tree diameter.

In the context of tree TOF acoustic measurement with a test span of 1.2 m, the wave propagation in a tree trunk can be in one of the following modes: 1) one-dimensional plane waves when tree diameter $D_i \leq 10$ cm, 2) transitional waves when tree diameter 10 cm $< D_i < 40$ cm, and 3) dilatational waves when tree diameter $D_i \geq 40$-cm.

Wave Velocity in Relation to Tree Diameter

The wave propagation velocities (V_i) in tree model 1 can be determined from the propagation distance (L_i) and the corresponding fastest arrival times (t_i) derived from the numerical simulations. In this study, wave velocity was calculated for a propagation distance of 1.2 m, which corresponds to the tree TOF measurement over the same test span. Figure 5 shows the relationship between the simulated tree acoustic velocity for the 1.2-m propagation distance and tree diameter (D_i). The simulation results indicate that wave velocity has a nonlinear relationship with tree diameter because of the changing wave behavior observed. The velocity
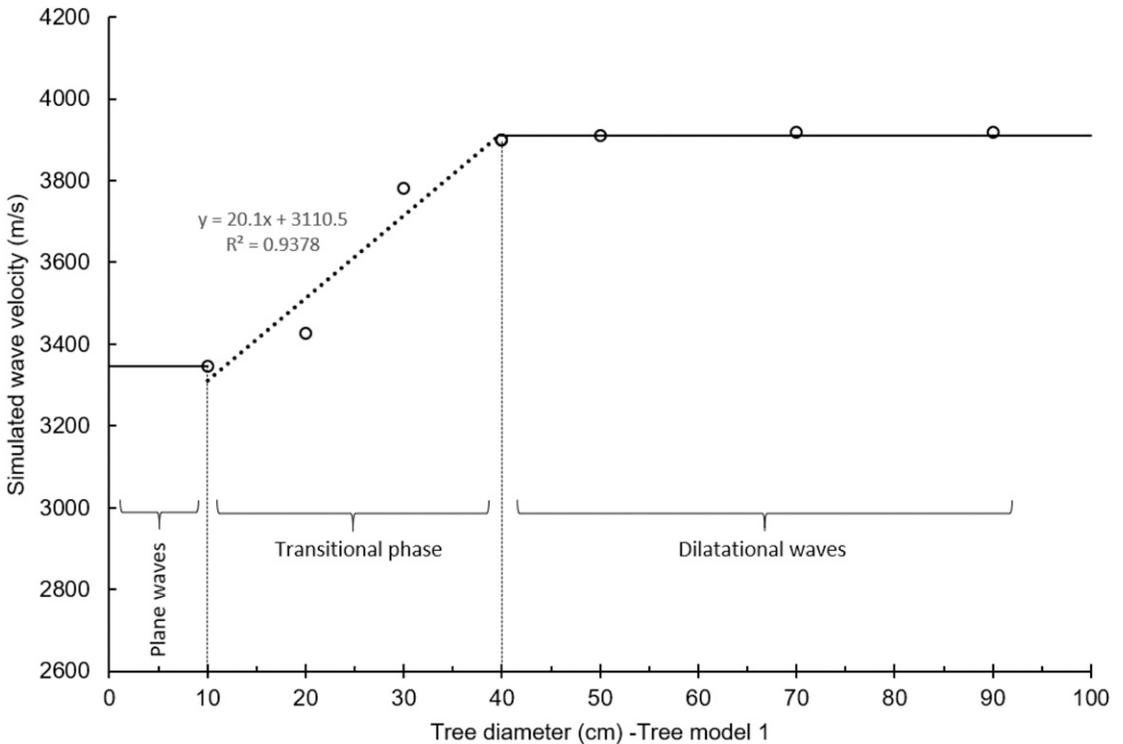
Figure 5. Relationships between simulated tree acoustic velocity for the 1.2-m propagation distance and tree diameter.

and diameter relationships can be characterized using three-segmented mathematical models:

$D_i \leq 10$ cm. The wave propagation patterns in Fig 4(a) indicate that when $D_i = 10$ cm, the wave propagation for the 1.2-m propagation distance is dominated by quasi-plane waves. This observation is supported by the wave velocity data obtained from the simulation run being very close to the theoretical velocity (3335 m/s) of one-dimensional plane wave. A simulation check for $D_i = 5$ cm resulted in a wave velocity (3345 m/s) that is also equivalent to the one-dimensional plane wave velocity. Therefore, it can be inferred that the wave propagates in a plane wave for tree models of $D_i \leq 10$ cm, and the following one-dimensional wave equation can be applied:

$$V_i = C_0, D_i \leq 10 \text{ cm.} \quad (4)$$

The implication of this finding is that the acoustic velocity measured on standing trees of 10 cm in

dbh or less can be treated as one-dimensional wave velocity and therefore is comparable to the log velocity measured using the acoustic resonance tool.

$10 < D_i < 40$ cm. When the tree diameter falls in the range of 10 cm and 40 cm, the wave propagation within the 1.2-m distance is neither in the plane wave mode nor in dilatational wave mode (Fig 4[b] and [c]). We consider this case as a transitional phase where tree acoustic velocity increases as tree diameter increases (Fig 5). A linear regression model can be used to describe the wave behavior in this transitional phase.

$$V_i = 3110.5 + 20.1D_i, \quad 10 < D_i < 40 \text{ cm.} \quad (5)$$

$D_i \geq 40$ cm. When the tree diameter reaches 40 cm, the wave propagation became dominated by dilatational waves, as shown in Fig 4(d)-(g). The wave propagated at a velocity of 3911 m/s

based on simulation runs, and the velocity remained relatively constant as the tree diameter increased from 40 cm to 90 cm. This simulated velocity is equivalent to the theoretical velocity of a dilatational wave ($C_L = 3935$ m/s) calculated from the average elastic constants and density of the green larch specimens (Liu et al 2015) using the three-dimensional wave equation (Eq 2). Consequently, the acoustic velocity measured on standing trees of 40 cm in diameter and larger should be treated as dilatational wave velocity.

$$V_i = C_L, \quad D_i \geq 40 \text{ cm}. \qquad (6)$$

Wave Velocity in Relation to Tree Slenderness

The effect of tree diameter on wave velocity can also be illustrated using the parameter of tree slenderness ratio such that the resulting relationships can be applied to situations where a different measurement span is used. The tree slenderness ratio (λ) is defined as the ratio of propagation distance (or test span) and tree diameter (D_i).

$$\lambda = L_i / D_i. \qquad (7)$$

Figure 6 shows the relationships between wave velocity and tree slenderness for $\lambda = 1.33$ to 24. Similarly, the relationships can be characterized using three-segmented mathematical models:

1. When tree slenderness $\lambda \geq 12$, waves propagate as quasi-plane waves, and thus the one-dimensional wave equation can be applied. Wave velocity remained constant and equivalent to "rod" velocity.

$$V_i = C_0, \lambda \geq 12. \qquad (8)$$

2. When tree slenderness $\lambda = 3\text{–}12$, waves propagate in the transitional mode. Wave velocity increases nonlinearly as tree slenderness decreases. The relationship between wave velocity and slenderness can be best characterized by the following mathematical model:

$$V = 3973.3(\text{Ln}\lambda)^{-0.203}, \quad 3 < \lambda < 12. \qquad (9)$$

3. When slenderness $\lambda \leq 3$, waves propagate as dilatational waves, and thus three-dimensional wave equation can be applied. Wave velocity remained relatively constant and equivalent to dilatational velocity.
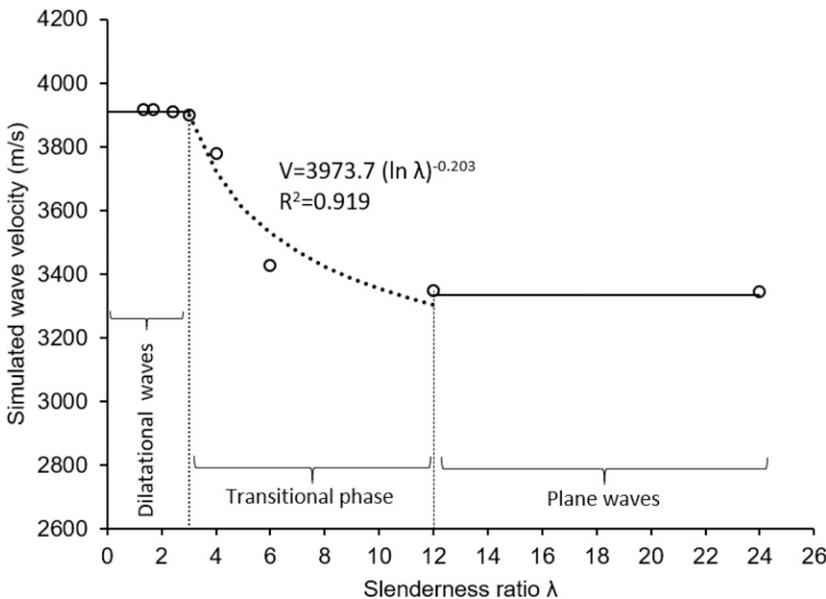

Figure 6.   Relationship between simulated tree velocity and the slenderness of tree trunk.

$$V_i = \ C_L, \lambda \leq 3. \qquad (10)$$

These results further validated the hypotheses on wave propagation on standing trees: first, when tree diameter is 10 cm or less, or slenderness $\lambda \geq 12$, the TOF velocity measured on standing trees can be treated as one-dimensional wave velocity and therefore is comparable to the log velocity measured using acoustic resonance tools. Second, when tree diameter is 40 cm or greater, or slenderness $\lambda \leq 3$, the TOF velocity measured on standing trees can be treated as dilatational wave velocity and therefore is not comparable to the log velocity measured using acoustic resonance tools. In this case, three-dimensional wave equation should be considered for wood property prediction instead of one-dimensional wave equation. Third, when tree diameter falls between 10 and 40 cm, or slenderness falls between 3 and 12, the TOF velocity measured on trees can neither be interpreted as one-dimensional wave velocity nor be interpreted as three-dimensional wave velocity; instead, the measured tree velocity should be adjusted based on the mathematical models developed before it can be analyzed for wood property prediction.

EFFECT OF JUVENILE WOOD ON WAVE PROPAGATION

Figure 7 shows wave propagation patterns in *Tree Model 2* ($D_i = 35$ cm) with the juvenile wood content in 40%, 50%, 60%, 70%, 80%, and 90%. In all these scenarios, the waves propagated in a very similar pattern. The obvious difference is that the wave propagation was slowed as the juvenile wood content increased. For instance, at $t = 500$ μs, the wave front traveled the longest distance (2.0 m) when the juvenile wood content was 40%; as the proportion of juvenile wood increased, the distance that the wave traveled gradually decreased, thus the wave velocity decreased.

Figure 8 shows the relationship between simulated wave velocity and the juvenile wood content in *Tree Model 2*. The wave velocities were determined based on the fastest arrival time (t_0) at 1.2-m propagation distance. A regression analysis indicated a negative linear relationship between wave velocity and proportion of juvenile wood ($R^2 = 0.98$). As the juvenile wood content increased from 40 to 90%, the corresponding acoustic wave velocity reduced from 4000 m/s to 3440 m/s. The linear regression model indicated that a 10% increase in the juvenile wood content
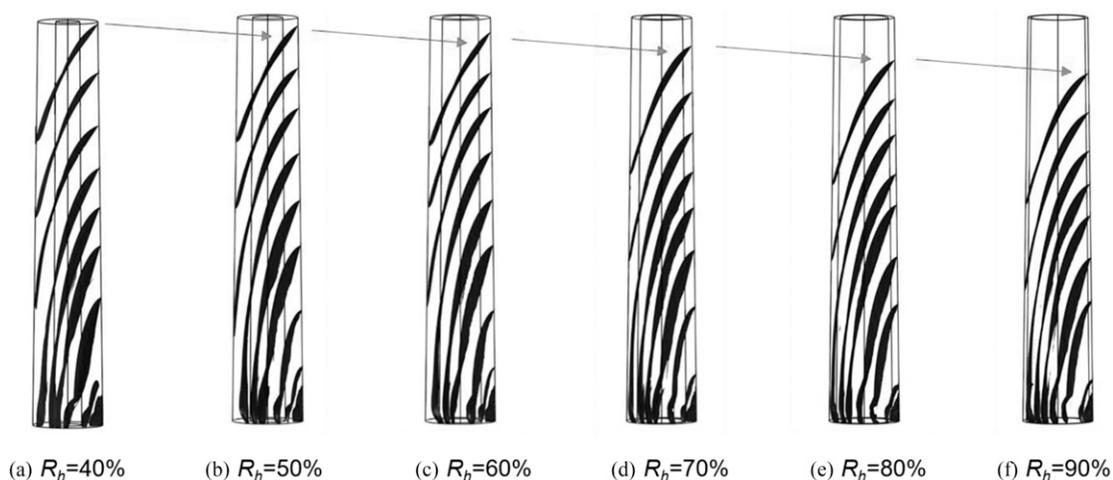

(a) R_h=40%   (b) R_h=50%   (c) R_h=60%   (d) R_h=70%   (e) R_h=80%   (f) R_h=90%

Figure 7.   Wave-front maps of Tree Model 2 with juvenile wood ranging from 40% to 90% ($t = 100$, 150, 200, 250, 300, 350, 400, 450, and 500 μs).
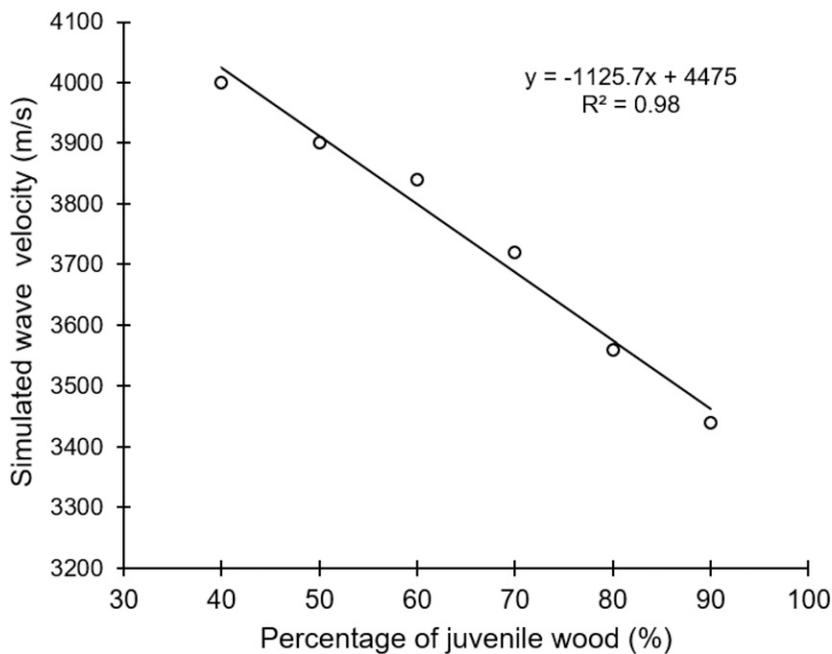
Figure 8.   Relationship between acoustic wave velocity in trees and proportion of juvenile wood.

could result in 113 m/s reduction in acoustic velocity. This velocity reduction is attributed to the lower stiffness and higher microfibril angel in the juvenile wood than those in the mature wood. When the proportion of juvenile wood increased, the low wood properties (primarily stiffness) of the juvenile wood negatively affected the wave propagation by dragging the entire wave front, resulting in a reduced wave propagation velocity, as shown in Fig 8.

Similar argument can also be made with respect to mature wood effect. As the proportion of mature wood increased in a tree's cross section (opposite trend with juvenile wood), the higher wood properties of mature wood positively affected the wave propagation by advancing the wave front, both in the mature wood zone and juvenile wood zone, thus resulting in an increase in wave velocity. This finding is a further evidence that wave propagation in standing trees is controlled by the wood properties of entire cross section, and the wave velocity measured on standing trees reflects the global properties of the wood between the two measuring points (1.2-m

span), not just the outerwood on the propagation path.

Although our simulation results demonstrated the effect of juvenile wood on TOF velocity of standing trees, this is not to say that juvenile wood equally affects wave propagation as the mature wood does. In fact, previous studies have reported that TOF velocities measured on standing trees are sensitive to the high localized stiffness of the outerwood (Chauhan and Walker 2006; Grabianowski et al 2006). This observation is supported by the wave propagation patterns in Figs 4 and 7 where the leading edges of the wave fronts have always been located in the outerwood and are used to determine the time of arrival at the stop probe over a propagation distance.

The wave propagation simulations in this study were carried out in tree models with two distinctly different wood zones, mature wood and juvenile wood, with each treated as homogenous and orthotropic. The natural property variation within each wood zone and gradual transition between

mature wood and juvenile wood were not modeled. But the simulation results should provide valid insight into the wave propagation behavior which helps to understand the impact of various factors (at levels of individual trees, stands, genetics, and environmental conditions) on tree acoustic measurements, and develop wood property prediction models using measured wave velocity and tree/stand parameters.

CONCLUSIONS

In this article, we investigated the effects of tree diameter and proportion of juvenile wood on wave propagation patterns and wave velocity in standing trees through numerical simulations. Based on the simulation results and analysis, we conclude the following:

1. Acoustic wave propagation in trees is dependent on both tree diameter and propagation distance. The acoustic waves generated through an impact initially spread over the cross section from the impact source as a dilatational wave, and the waves then enter into a transitional phase with tilted wave fronts and eventually change to quasi-plane waves and pure plane waves.

2. With respect to TOF acoustic measurement on standing trees, wave propagation in a tree trunk within the typical test span can be classified into three different modes: 1) when tree diameter $D \leq 10$ cm or slenderness $\lambda \geq 12$, wave propagates as quasi-plane waves; the TOF velocity measured on trees can be treated as one-dimensional wave velocity and therefore is comparable to the log velocity measured using the acoustic resonance method; 2) when tree diameter $D \geq 40$ cm or slenderness $\lambda \leq 3$, wave propagates as dilatational waves; the TOF velocity measured on trees is not comparable to the resonance velocity. In this case, the three-dimensional wave equation should be considered for wood property prediction; 3) when tree diameter falls between 10 and 40 cm or slenderness falls between 3 and 12, wave propagation is in a transitional phase. TOF velocity in this mode is higher than resonance velocity, but lower than dilatational wave

velocity. Mathematical models can be used to convert the TOF velocity in the transition mode to resonance velocity.

3. The increase in the juvenile wood content does not seem to change the wave propagation patterns, but it slows the wave propagation. Our simulation results indicated that a 10% increase in the juvenile wood content could result in a 113 m/s reduction in acoustic velocity. This velocity reduction is attributed to the lower stiffness and higher microfibril angle in the juvenile wood than those in the mature wood.

4. The simulation results of this study do not support the speculations that the TOF method used on standing trees only measure the wave velocity of the outerwood, which lead to questions on the effectiveness of the TOF method for tree quality assessment. Instead, our results indicated that wave propagation in standing trees is controlled by the wood properties of entire cross section, not just the outerwood. Therefore, the wave velocity measured on standing trees reflect the global properties of the wood between the two measuring points. Further research should include physical testing to validate the findings.

REFERENCES

Andrews M (2003) Which acoustic speed? Pages 156-165 *in* Proceedings of the 13th International Symposium on Nondestructive Testing of Wood, August 19-21, 2002, University of California Berkeley, Berkeley, CA.

Carter P, Briggs D, Ross RJ, Wang X (2005) Acoustic testing to enhance western forest values and meet customer wood quality needs. Productivity of western forests: A forest products focus. Gen Tech Rep PNW-GTR-642. USDA For Serv Pacific Northwest Research Station, Portland, OR. pp. 121-129.

Chauhan SS, Walker JCF (2006) Variation in acoustic velocity and density with age, and their interrelationships in radiata pine. For Ecol Mgmt 229(1-3):388-394.

Grabianowski M, Manley B, Walker JCF (2006) Acoustic measurements on standing trees, logs and green lumber. Wood Sci Technol 40(3):205-216.

Hsu CY (2003) Radiata pine wood anatomy structure and biophysical properties. PhD thesis, School of Forestry, University of Canterbury, Christchurch, New Zealand. 147 pp.

Joe B, Dickson R, Raymond CA (2004) Prediction of *Eucalyptus dunnii* and *Pinus radiata* timber stiffness using acoustics. RIRDC Publication. 04/013. 121 pp.

Lasserre JP, Mason EG, Watt MS (2004) The influence of initial stocking on corewood stiffness in a clonal experiment on 11-year-old *Pinus radiata* [D. Don]. N Z J Sci 49:18-23.

Lindström H, Harris P, Nakada R (2002) Methods for measuring stiffness of young trees. Holz Roh-Werkst 60: 165-174.

Liu F, Jiang F, Zhang J, Zhang H (2015) Twelve elastic constant values of larch forest. Xibei Linxueyuan Xuebao 30(6):227-231.

Liu F, Wang X, Zhang H, Jiang F, Yu W, Liang S, Fu F, Ross RJ (2020) Acoustic wave propagation in standing trees – Part 1. Numerical simulation. Wood Fiber Sci 52(1):53-72.

Legg M, Bradley S (2016) Measurement of stiffness of standing trees and felled logs using acoustics: A review. J Acoust Soc Am 139(2):588-604.

Meyers MA (1994) Dynamic behavior of materials. Wiley, New York, NY.

Mora CR, Schimleck LR, Isik F, Mahon JM, Clark A, Daniels RF (2009) Relationship between acoustic variables and different measures of stiffness in standing *Pinus taeda* trees. Can J Res 39(8):1421-1429.

Wang X (2013) Acoustic measurements on trees and logs: A review and analysis. Wood Sci Technol 47(5):965-997.

Wang X, Carter P, Ross RJ, Brashaw BK (2007a) Acoustic assessment of wood quality of raw forest materials–A path to increased profitability. Forest Prod J 57(5):6-14.

Wang X, Ross RJ, Brashaw BK, Punches J, Erickson JR, Forsman JW, Pellerin R (2004) Diameter effect on stress-wave evaluation of modulus of elasticity of logs. Wood Fiber Sci 36(3):368-377.

Wang X, Ross RJ, Carter P (2007b) Acoustic evaluation of wood quality in standing trees. Part I. Acoustic wave behavior. Wood Fiber Sci 39(1):28-38.